ELSEVIER

Materials Science and Engineering B 134 (2006) 125–129

MATERIALS SCIENCE & ENGINEERING B

www.elsevier.com/locate/mseb

Structure of biomembrane-on-silicon hybrids derived from X-ray reflectometry

M. Birkholz [a,*], P. Zaumseil [a], M. Kittler [a], I. Wallat [b], M.P. Heyn [b]

[a] *IHP, Im Technologiepark 25, D-15236 Frankfurt (Oder), Germany*
[b] *Fachbereich Physik, FU Berlin, Arnimallee 14, D-14195 Berlin, Germany*

Received 4 May 2006; received in revised form 30 June 2006; accepted 3 July 2006

Abstract

The organic–inorganic interface and its proper structural adjustment are of central importance for the fabrication of hybrid material systems from biomolecules and semiconductors. Such material hybrids are currently under development for several advanced applications, in particular for biomolecular sensing. An investigation of biomolecular immobilization on semiconductor surfaces by X-ray reflectometry (XRR) will be presented. Complete biomembrane patches of purple membrane (PM) from *Halobacterium salinarum* were immobilized on oxidized and nitrided silicon wafers. A covalent immobilization protocol based on 3-aminopropyltriethoxysilane (APTS) and glutaric dialdehyde (GD) was applied for cross-linking the biomolecules to the semiconductor surface. XRR could be shown to yield the relevant morphological parameters of biomolecular monolayers such as layer thickness, interface roughness and coverage. Synchrotron radiation was not required, but a laboratory rotating anode set-up was sufficient to study the prepared stacking of organic monolayers. According to the measurement and analysis of XRR patterns both cross-linking layers APTS and GD are required for bonding purple membrane patches to SiO_2/Si, whereas GD alone suffices for cross-linking to Si_3N_4/Si. This distinct behavior offers a pathway for nanopatterning of biomolecules on Si surfaces by selective passivation.
© 2006 Elsevier B.V. All rights reserved.

Keywords: Biomolecular monolayer; Purple membrane; Si wafer; X-ray reflectometry; Bacteriorhodopsin

1. Introduction

The continuous shrinking of minimum feature dimensions in microelectronics into the sub 100 nm range has taken semiconductor devices to ever closer approach the spatial dimensions of biomolecular materials and their complex 3D assemblies like proteins, fibrils, carbohydrates, biomembranes and other biological nanocomposites. The biomolecule-semiconductor interface and its proper structural adjustment is a central issue for hybrid material systems that are currently under development for several applications like biomolecular sensing [1–3], optoelectronics [4] and molecular computing [5]. The development of complex hybrid multilayers requires the availability of laboratory-based techniques for the determination of the structure and morphology of all layers involved. In this work an investigation will be presented of biomolecular immobilization on standard semiconductor surfaces by X-ray reflectometry (XRR) with a laboratory diffractometer.

The XRR technique has been introduced for the investigation of single thin inorganic films on smooth substrates [6] and was later applied to the detection of surface chemical reactions and the analysis of multilayers [7]. The technique essentially probes the electron density ρ_e and thickness t of surface layers, but is also sensitive to surface and interface roughness σ that may be included – in its simplest form – by a Debye–Waller factor like effective damping term [7,8]. The number of XRR investigations of thin inorganic layers has exploded in the last decade due to the increasing availability of (i) parallel beam optics for conventional powder diffractometers [9] and (ii) synchrotron radiation with XRR-dedicated beam lines. The high intensity available with synchrotron radiation also enabled the investigation of organic and biological layers, the XRR analysis of which is generally impeded by their low electronic density. Recent XRR studies with synchrotron radiation were concerned with the so-called unbinding transition of phospholipid membranes [10], processes of induced crystallization [11,12] or prevention

* Corresponding author.
E-mail address: birkholz@ihp-microelectronics.com (M. Birkholz).

0921-5107/$ – see front matter © 2006 Elsevier B.V. All rights reserved.
doi:10.1016/j.mseb.2006.07.001

Table 1
Assumed XRR simulation parameters for the materials considered in this work; critical angles θ_c are specified for usage of Cu Kα radiation

Material	Stoichiometry	Mass density (g cm^{-3})	Electron density, ρ_e (nm^{-3})	Critical angle, θ_c (°)
Silicon	Si	2.33	699	0.223
Silicon dioxide	SiO_2	2.20	662	0.217
Silicon nitride	Si_3N_4	3.20	961	0.261
3-Aminopropyltriethoxysilane	$C_9H_{23}NO_3Si$	0.949	315	0.149
Glutaric dialdehyde	$C_5H_8O_2$	1.06	345	0.149
Purple membrane	$\sim C_{74}H_{140}\ N_{14}O_{21}PNa$	1.35	441	0.176

of protein unfolding by cross-linking at the gas–water interface [13], polymer surface gratings [14], the structural order of organic-on-inorganic semiconductors [15] and the increase of organic layer stability by capping with aluminum oxide [16] to mention only a few examples. Further details of the XRR technique are outlined, for instance, in Refs. [17] or [9].

In this work, layers of SiO_2 and Si_3N_4 on Si wafers were selected as the relevant substrate materials, since both surfaces represent fundamental terminations in CMOS (complementary metal-oxide semiconductor) technology. A widely used immobilization procedure was applied that makes use of a cross-linking protocol based on 3-aminopropyltriethoxysilane (APTS) and glutaric dialdehyde (GD) [2,18,19]. The working principle of this two-step cross-linking procedure is to convert the initial Si–OH terminated surface to amino groups—NH_2 and subsequently aldehyde groups—CHO, the latter of which bind to the protein. Complete patches of so-called purple membrane (PM) from *Halobacterium salinarum* comprising the bacterial proton-pump bacteriorhodopsin as integral membrane protein, were selected as biomolecules to be immobilized on oxide covered and nitride covered Si wafers. Purple membrane patches have a thickness of about 5.6 nm and an average lateral dimension of some 100 nm.

2. Experimental

B-doped CZ-Si wafers of (0 0 1) orientation, 200 mm diameter and 575 μm thickness with 20–60 Ω cm were used as substrates. Cover layers of SiO_2 and Si_3N_4 with an intentional thickness of 5 nm were prepared by thermal oxidation at 800 °C and chemical vapor deposition at 690 °C, respectively. Pieces of 40 mm × 40 mm were cut from the wafers after discharging from the IHP clean room. Immobilization experiments were performed by consecutively exposing the oxide or nitride covered Si plates to solutions of APTS, GD and purple membrane patches (PM). APTS and GD were purchased from Sigma and diluted to 6.6 vol.% in Cl_3CH and 0.4 mM in H_2O, respectively. Ultrapure water from Millipore was used for all washing and dilution procedures (MilliQ PF-plus, >18.2 MΩ). Purple membrane patches were harvested from the ET1001 strain (wild type, formerly S9) and diluted to contain 0.75 μM bacteriorhodopsin. Reaction times were set to 2, 10 and 60 min for solutions of APTS, GD and PM, respectively, while the samples were rinsed in water, or Cl_3CH in case of APTS, after each reaction. After the preparation was finished the hybrid samples were kept in a high-humidity atmosphere in order to avoid dehydration of purple membrane patches, which are known to structurally deteriorate at low humidity. The XRR properties of materials used are given in Table 1.

Measurements of X-ray reflectivity were performed with a rotating anode diffractometer set-up (Rigaku RU 300) and applying Cu Kα radiation. The generator was operated under 20 kV/10 mA or 50 kV/150 mA during the measurement according to whether the scattering angle range was scanned up to 2° or between 1.5° and 10°. This procedure avoided damage to the detector due to the high reflectivity in the vicinity of the critical angle. The scattered X-ray beam was monochromatized before entering the detector by a graphite monochromator of (0 0 0 2) orientation. Albeit the diffractometer operates in the widely used para-focussing mode, a quasi-parallel beam setting was achieved by choosing the smallest divergence slit available of only 0.05°. This in-scattering-plane divergence translates into a beam height of 0.16 mm at the sample center position (R_{diff} = 185 mm). During the XRR measurement the sample was exposed to a saturated humidity atmosphere that was contained in the sample housing by closing the windows with an X-ray transparent plastic foil (4 μm Trespaphan). Reflectivity scans between 0.1° and 10° were collected with a step size of 0.01° and an integration time of 2 s for low and medium scattering angle range. The analysis of XRR pattern was performed by virtue of the reflectivity simulation and regression program RCRefSim [20].

3. Results and discussion

Fig. 1 shows the measured XRR patterns of the SiO_2/Si sample (bottom) and the same sample subjected to the immobilization protocol (top), i.e. having purple membrane patches intentionally attached to the SiO_2 surface via cross-linking with APTS and GD. Dots represent measured data points, while solid lines indicate simulations according to layer architecture models as outlined below.

The pattern from the oxide covered wafer, Fig. 1 (bottom) is realized to span an intensity range of about seven orders of magnitude. Although a thickness of the oxide of only 5 nm was intended a reliable fit to the data could only be obtained by modeling the SiO_2 layer with a thickness of 5.5 nm and an effective (root-mean-square, rms) roughness of 0.34 nm. The relative density exceeded the theoretical value of 2.33 g/cm^3 by 6%. Errors are given for the last digits by numbers in parentheses. The reliability value S_1 of the numerical regression decreased further by introducing a surface layer of low electron density and only

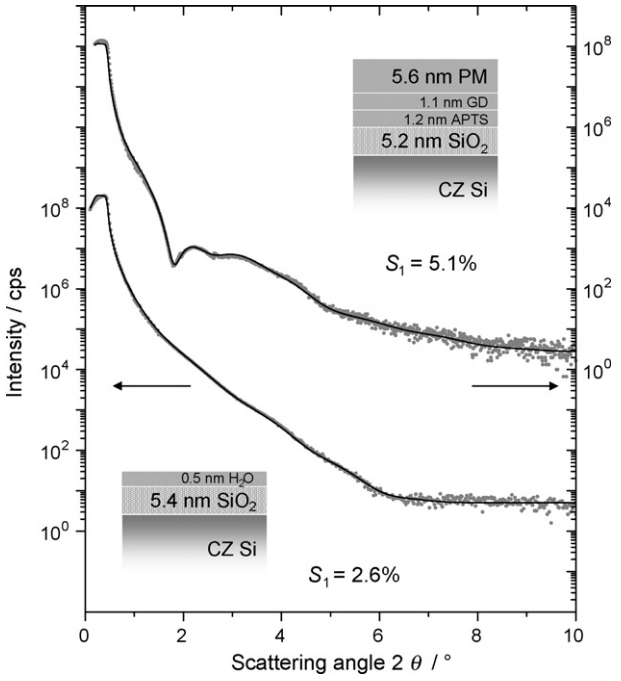

Fig. 1. Measured (gray dots) and simulated XRR pattern (black lines) of SiO_2/Si (bottom) and PM/GD/APTS/SiO_2/Si (top).

0.5 nm thickness on top of the SiO_2, which could either indicate a water layer or a silicon-hydroxide surface monolayer upon the oxide film. A rather small S_1 value of 2.6% was finally achieved.

The XRR pattern of the oxide sample with intentionally immobilized PM patches, given in Fig. 1 (top), exhibits a distinctively different course of intensity than the pure oxide sample although no well-pronounced Kiessig fringes are observed. The analysis of the pattern was performed by subjecting all possible layer architectures that might have been formed to a numerical regression. If SiO_2, APTS, GD and PM are further abbreviated by characters O, A, G and P, the seven layer systems O, AO, GAO, PGAO, PGO, PAO and PO might have been prepared in principle. Here, the top layer is given as the first character. For instance, GAO stands for the GD/APTS/SiO_2/Si multilayer model, while O would account for an uncovered SiO_2/Si sample with completely absent APTS, GD and PM layers. For all seven-layer models reliable starting parameters were inserted into the simulation program in order to identify a small-S_1 fit to the measured data. The electron densities given in Table 1 were used for this purpose. Fit models were rejected for implausible fit parameters, which were assumed of having arrived at when either the electron density surmounted the values given in the table by more than 50%, when the roughness of a layer σ increased over its thickness t or when the final S_1 value exceeded 20%.

On the basis of these criteria the intended layer architecture of PGAO turned out as the one with the smallest S_1 value of 5.1% and the most reliable fit parameters. Alternative models like AO, GAO and GO yielded S_1 values of 8.7%, 7.9% and 17.3% in combination with implausible parameter values. It can be concluded that the regression of the measured data yielded in fact the intended layer stacking of purple membrane patches bonded to the SiO_2/Si substrate via cross-linking molecules GD and APTS. The parameters of the best-fit model architecture are given in Table 2 and partially in Fig. 1, where the solid line is calculated on the basis of this model. The relative density in the table accounts for the fitted electron density ρ_e in fractions of the theoretical density specified in Table 1.

The numerical results presented in Table 2 shall now be discussed. Firstly, the oxide layer parameters were fixed to the values obtained from the fitting of the SiO_2/Si sample without the water layer on top. Secondly, the relative density of the APTS layer exceeds by 20% the value it attains in solution. This might be a reliable result, since APTS molecules are generally considered to vertically bond to the SiO_2 surface and, moreover, to horizontally cross-link to molecular neighbors, which will be associated with a density increase of a surface-bonded monolayer of APTS. Thirdly, the thickness of the GD layer is realized to exceed the lengths of the GD molecule of about 1 nm. This might be understood from the ability of GD to form some multilayer thick polymers upon APTS due to the symmetric functional –CHO groups of the molecule [2]. A further point of interest relates to the relative density of the PM layer that translates into coverage of about 23%. A less than complete coverage has been observed in various other investigations that made use of the APTS-GD cross-linking scheme [1,18]. Finally, the value for the PM layer thickness of 5.6 nm is in good agreement with literature values. It can thus be concluded that the thickness and relative density values of the model architecture yielded reliable results that are in accordance with previous investigations by other techniques than XRR.

Reflectometry patterns of the nitrided wafer prior to and after immobilization are shown in the bottom and top of Fig. 2. Both measurements yielded clearly visible Kiessig fringes that are mainly caused by the 6.4 nm thin nitride layer the electron density of which differs by about 50% from the underlying Si wafer, see Table 1. This is in strong contrast to the SiO_2/Si system, where the electron density difference between surface layer and substrate is only in the 5% range. Subjecting the Si_3N_4/Si wafer to the APTS-GD-PM immobilization procedure yielded an XRR pattern that appears comparable to the wafer prior to immobilization, compare Fig. 2. Various numerical simulations, however, reveal that purple membrane patches have covalently been bonded to the surface via an intermediate glutaric dialdehyde layer. The architecture of the best-fit PGN model is shown as inset in Fig. 2. As for the oxide system various model systems like N, AN, GN, GAN, PN, PGN, PAN and PGAN were tested to fit the measured data, where N stands for the nitride

Table 2
Layer architecture parameters of the best-fit model for PM immobilization on SiO_2/Si

No.	Layer	Thickness (nm)	Roughness (nm)	Relative density
1	PM	5.6	0.8	0.23
2	GD	1.1	0.6	1.06
3	APTS	1.2	0.1	1.21
4	SiO_2	5.2	0.3	1.07
5	Si substrate	∞	0.2	1.00

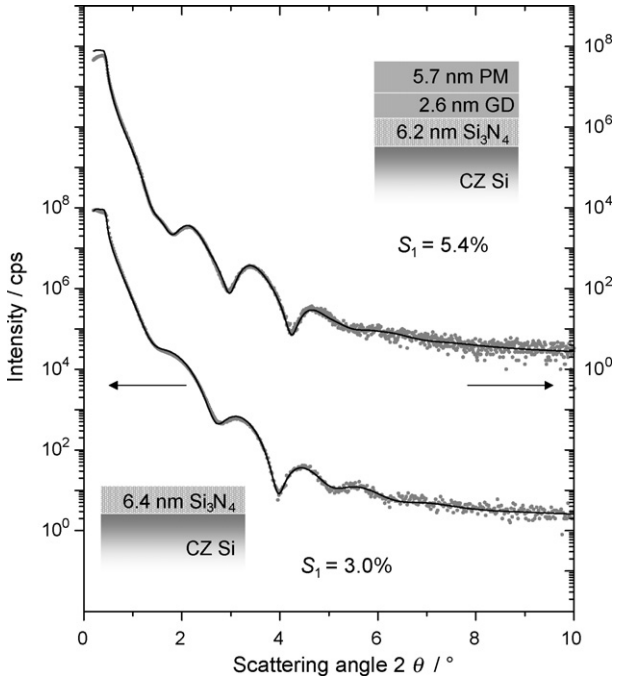

Fig. 2. Measured (gray dots) and simulated XRR pattern (black lines) of Si_3N_4/Si (bottom) and PM/GD/Si_3N_4/Si (top).

Si_3N_4 layer and the other symbols have the same meaning as explained above. In case of a silicon dioxide coating the application of the procedure would have led to a PM/GD/APTS layer architecture, but the usage of a nitride coated wafer results in a PM/GD stack directly bound to the Si_3N_4 layer. Different models like PGAN or GN yielded significantly larger S_1 values. The numerical values of the final fit PGN model are given in Table 3.

This result may be explained by assuming that APTS does not bond to the Si_3N_4 surface. On the other hand, the connection between PM patches and the nitride can be achieved through cross-linking with GD. Accordingly, the immersion step of nitrided wafers in APTS may be omitted, since the immobilization may already be achieved by cross-linking with GD alone. This is naturally understood from the nitrogen termination of the Si_3N_4 surface to which glutaric dialdehyde may covalently bond. The same bonding scheme is made use of by converting the SiO_2 surface with APTS to a nitrogen-terminated surface. This reduced cross-linking scheme for nitrided surfaces was verified by succeeding experiments, where PM was immobilized after cross-linking with GD only. And, in fact, the XRR pattern obtained yielded the smallest S_1 values when modeled by PM/GD/Si_3N_4/Si. It is concluded that purple membrane patches may be immobilized on nitrided silicon surfaces by cross-linking with glutaric dialdehyde only. This result may also apply to other biomolecules than complete PM patches and may offer a strategy for the surface patterning of semiconductor surfaces with biomolecules.

Table 3
Layer architecture parameters of the best-fit model for PM immobilization on Si_3N_4/Si

No.	Layer	Thickness (nm)	Roughness (nm)	Relative density
1	PM	5.7	0.7	0.25
2	GD	2.6	0.7	1.14
3	Si_3N_4	6.2	0.5	0.90
4	Si substrate	∞	0.1	1.00

4. Conclusions

The immobilization of complete purple membrane patches on SiO_2 and Si_3N_4 terminated Si wafer surfaces have successfully been demonstrated by a covalent cross-linking scheme. X-ray reflectometry was found to be capable of probing even monolayers of biomolecules, albeit only a laboratory set-up was used instead of synchrotron radiation that is more commonly applied for thin films containing low-*Z* elements. The determination of biolayers became possible through the usage of a high-intensity rotating anode and the quasi-parallel beam configuration, i.e. the usage of a very small divergence slit. Important structural and morphological parameters of biomolecular immobilization like layer thickness and interface roughness may then be obtained. Moreover, the obtained relative density may be interpreted as surface coverage and XRR thus allows for the quantitative determination of efficiency of immobilization procedures. It can thus be concluded that a complicated layer architecture has successfully been elucidated here. It has to be emphasized, however, that a reliable analysis and interpretation of XRR patterns from complex multilayer systems always has to be performed on a firm modeling basis, i.e. the structure determination is always a decision between distinct alternative structure models rather than the structure is determined in an *ab initio* approach. Comparing XRR and optical ellipsometry, the first method directly yields the layer thickness; whereas only the effective layer thickness – which is the product of the refractive index and layer thickness – is achieved by the second technique. The advantage of XRR for thin film analysis is caused by the small deviation of the refractive index from unity. The investigation has shown that biomembrane patches may covalently be bound to SiO_2/Si by cross-linking with APTS and GD and to Si_3N_4/Si by using GD alone. This distinct immobilization behavior should allow for the patterning of biomolecules on semiconductor surfaces by selective passivation.

Acknowledgements

The authors like to thank the staff from the IHP pilot line for processing of the silicon wafers. This work has partially been supported by the Volkswagen-Stiftung through the SOBSI project (self-organized pattern formation of biomolecules at silicon surfaces, see www.mpi-halle.mpg.de/∼sobsi/home.htm).

References

[1] M. Thust, M.J. Schöning, J. Vetter, P. Kordos, H. Lüth, Anal. Chim. Acta 323 (1996) 115.
[2] A.K. Singh, A.W. Flounders, J.V. Volponi, C.S. Ashley, K. Wally, J.S. Schoeniger, Biosens. Bioelectr. 14 (1999) 703.
[3] R. Hölzel, F.F. Bier, AIP Conf. Proc. 725 (2004) 77.
[4] P. Bhattacharya, J. Xu, G. Váró, D.L. Marcy, R.R. Birge, Opt. Lett. 27 (2002) 839.

[5] C.P. Collier, E.W. Wong, M. Belohradský, F.M. Raymo, J.F. Stoddart, P.J. Kuekes, R.S. Williams, J.R. Heath, Science 285 (1999) 391.
[6] H. Kiessig, Ann. Phys. 10 (1931) 769.
[7] L.G. Parratt, Phys. Rev. 95 (1954) 359.
[8] S.K. Sinha, E.B. Sirota, S. Garoff, H.B. Stanley, Phys. Rev. B 38 (1988) 2297.
[9] M. Birkholz, Thin Film Analysis by X-ray Scattering, Wiley-VCH, Weinheim, 2006 (Chapter 4).
[10] M. Vogel, C. Münster, W. Fenzl, T. Salditt, Phys. Rev. Lett. 84 (2000) 390.
[11] K. Larson, D. Vaknin, O. Villavicencio, D. McGrath, N. Stephenson, V.V. Tsukruk, Polym. Mater.: Sci. Eng. 85 (2001) 229.
[12] D. Vaknin, S. Dahlke, A. Travesset, G. Nizri, S. Magdassi, Phys. Rev. Lett. 93 (2004) 218302.
[13] D. Gidalevitz, H. Zhengqing, S.A. Rice, Proc. Natl. Acad. Sci. 96 (1999) 2608.
[14] T. Geue, M. Schultz, J. Genzer, U. Pietsch, A. Natansohn, P. Rochon, J. Appl. Phys. 87 (2000) 7712.
[15] A.C. Dürr, F. Schreiber, M. Münch, N. Karl, B. Krause, V. Kruppa, H. Dosch, Appl. Phys. Lett. 81 (2002) 2276.
[16] S. Sellner, A. Gerlach, F. Schreiber, et al., Adv. Mater. 16 (2004) 1750.
[17] P. Fewster, X-ray Scattering from Semiconductors, Imperial College Press, London, 2003.
[18] B. Schnyder, R. Kötz, D. Alliata, P. Facci, Surf. Interface Anal. 34 (2002) 40.
[19] T. Schiestel, H. Brunner, G.E.M. Tovar, J. Nanosci. Nanotech. 4 (2004) 504.
[20] P. Zaumseil, RCRefSim (rocking curve and reflectivity simulation), program available from the author (zaumseil@ihp-microelectronics.com) Frankfurt (Oder), 2005.